Document downloaded from:

http://hdl.handle.net/10251/201815

This paper must be cited as:

Iglesias, D.; Guerra, J.; Lucío, MI.; González-Cano, RC.; Lopez Navarrete, JT.; Ruiz Delgado, MC.; Vázquez, E.... (2020). Microwave-assisted functionalization of carbon nanohorns with oligothiophene units with SERS activity. Chemical Communications. 56(63):8948-8951. https://doi.org/10.1039/D0CC03496G

The final publication is available at

https://doi.org/10.1039/D0CC03496G

Copyright The Royal Society of Chemistry

Additional Information

Microwave-assisted functionalization of carbon nanohorns with oligothiophene units with SERS activity†

Daniel Iglesias, [a] Javier Guerra, [b] Mar´ıa Isabel Lucío, [c] Rafael C. Gonzâlez-Cano,[d] Juan T. Lõpez Navarrete,[d] M. Carmen Ruiz Delgado,[d] Ester Vâzquez [ef] and M. Antonia Herrero *[ef]

Carbon nanohorns have been functionalized with oligothiophene units *via* the 1,3-dipolar cycloaddition reaction under microwave irradiation and solvent-free conditions. A dramatic Raman enhancement was found for one of the synthesized derivatives. Experimental and *in silico* studies helped to understand the enhancement, attributed to the modification of electromagnetic fields upon functionalization at the tip of the nanostructures.

Nanotechnology burst onto the scene with the fast improvement of characterization techniques and the development of new nanomaterials. This multidisciplinary field is expected to overcome many of the most important challenges that the scientific community faces nowadays, such as the development of fast and reliable imaging. In this regard, surface-enhanced Raman spectroscopy (SERS) is a very powerful technique.[1] The absence of autofluorescence, the narrow spectral lines and the possibility to obtain multiple colors with a single excitation wavelength in a region with low background make Raman imaging an ideal choice in bio-imaging.[2] For instance, theG-mode of isotopically modified single-walled carbon nano- tubes (CNTs) was engineered and displayed three different colors in Raman imaging.[3] Two different effects, often called field enhancement (FE) and chemical enhancement (CE), are responsible for the magnification observed in SERS. FE, attributed to the interaction between an appropriate wavelength and metal particles or surfaces, shows greater enhancements than CE. CE results from the interaction between the material surface and the adsorbed molecule, usually involving electronic effects such as charge-transfer processes.[4] This factor depends on the electronic interaction between the adsorbate and the substrate, which requires a specific match at a single chemical site on the surface. CE is limited to very short distances. Additionally, resonance Raman enhancement is observed when the excitation wavelength falls within the electronic transition of the molecule (*e.g.* HOMO–LUMO).[5]

The finest material engineering techniques have allowed the development of very powerful SERS substrates. For instance, Bodelón *et al.* embedded plasmonic structures (*i.e.* Au nanorods, nanospheres or nanorod plasmonic crystals) in various matrices (*i.e.* a polymeric hydrogel, mesoporous TiO_2, or mesoporous SiO_2) to track pyocyanin down to 10^{-14} M, which allowed them to follow quorum sensing in bacterial films.[6] Nanomaterial synthesis and functionalization determine their performance. For instance, the so-called graphene-enhanced Raman scattering requires the precise synthesis of monolayer graphene. Otherwise, the enhancement decreases as the number of layers increases.[5] In another example, the Fermi energy (E_f) level of CVD graphene was tuned by introducing N atoms in the 2D lattice during the synthesis.[7] The modified E_f was closer to the LUMO orbitals of the analytes than the E_f of pristine graphene (*i.e.* without N atoms), which makes the charge-transfer process responsible for Raman enhancement easier, sensing rhodamine B down to 10^{-11} M. The latter and other studies show the potential of carbon nanomaterials in this field,[4,8,9] but only a few of them have reported the SERS effect in the absence of metals. Surprisingly, the potential of carbon nanohorns (CNHs)[10] has been scarcely investigated to date.

Further development of nanomaterials for Raman imaging and sensing will require a deep understanding of the systems. Recently, we reported, to the best of our knowledge, the first example of Raman enhancement using CNHs.[11] A series of di-, tri- and tetra-substituted oligothiophenephenylvinylene dendrons

[a] *Université de Strasbourg, CNRS, ISIS, 8 Allée Gaspard Monge, 67000 Strasbourg, France*

[b] *Facultad de Ciencias, Universidad de Valladolid, 47011, Valladolid, Spain*

[c] *Instituto Interuniversitario de Investigación de Reconocimiento Molecular y Desarrollo Tecnológico (IDM), Universitat Politècnica de València, Universitat de València, Camino de Vera s/n, 46022 Valencia, Spain*

[d] *Department of Physical Chemistry, University of Malaga, Campus de Teatinos s/n, Malaga 29071, Spain*

[e] *Facultad de Ciencias y Tecnologías Químicas, Universidad de Castilla-La Mancha (UCLM), 13071 Ciudad Real, Spain. E-mail: MariaAntonia.Herrero@uclm.es*

[f] *Instituto Regional de Investigacion Científica Aplicada (IRICA), 13071 Ciudad Real, Spain*

were non-covalently attached to CNHs. The substitution pattern of the molecules strongly influenced the molecule–CNH interaction. Thus, the tri-substituted dendrons interacted *via* p–p stacking, while CH–p interaction prevailed in the di- and tetra-analogues, which appeared to be bent around CNH to maximize the interaction. Interestingly, the latter showed a significantly higher Raman enhancement.

The possibility to induce SERS activity in nanomaterials with wide-ranging chemical characteristics is clear. In turn, the nanomaterial morphology is also a key factor. The subjecthas been largely explored for metal nano-assemblies,[12,13] yet scarcely investigated for carbon nanomaterials of different shapes. In this work, we have followed a fast, eco-friendly and scalable methodology to synthesize functionalized CNHs (f-CNHs) with thiophene units in a controlled manner. Three different derivatives have been used to evaluate the influence of functionalized CNHs when increasing the number of thiophene units. Characterization of the materials unequivocally showed covalent functionalization and revealed a significant Raman enhancement in certain derivatives, which makes them suitable candidates in the field of multi-color Raman imaging. Density functional theory (DFT) calculations were performed to study this phenomenon *in silico*. Besides, functionalized CNTs (f-CNTs) and non-covalently functionalized CNHs were prepared to assess the effect of the carbon nanostructure morphology and the nature of the interaction between the molecules and CNHs.

Functionalization of CNHs was achieved *via* 1,3-dipolar cycloaddition (Fig. 1 top). The reaction involves generation of azomethine ylides *in situ* upon thermal condensation of an a-amino acid and an aldehyde.[14,15] In this case, glycine and three different aldehydes with an increasing number of thiophene units (*i.e.* one, two or three units for aldehydes 1, 2 or 3, respectively) and CNHs were reacted under microwave irradiation and solvent-free conditions following the experimental conditions previously reported in our group.[15] The method provided functionalized CNHs with *N*-pyrrolidines substituted with the corresponding thienyl unit. The five-membered heterocycles were integrated covalently in the nanostructures. This increases their stability in contrast to the non-covalent f-CNHs, which rely on weaker supramolecular interactions (*e.g.* p–p stacking). In addition, the reproducibility of the applied synthetic method is superior to that of most non-covalent approaches. Both stability and reproducibility are important aspects that must be accomplished for the global implementation of SERS applications.[1] As the main drawback, covalent functionalization comes at the expense of the graphitic structure. Transmission electron microscopy confirmed that the unique structure of CNHs was not compromised (Fig. 1a, see Fig. S1, ESI† for the morphological characterization of p-CNH). The functionalization was established by thermogravimetric analysis (TGA) (Fig. 1b), which permitted the quantification of the degree of functionalization by comparing the thermal stability of p-CNH and f-CNHs at 550 1C. The calculated values were 866, 574 and 448 mmol g^{-1} for f-CNH 1, f-CNH 2 and f-CNH 3, respectively. The increase of defectiveness in the functionalized CNHs was assessed by Raman spectroscopy (Fig. 1c). Pristine CNHs (p-CNH) display a graphitic peak (G-band, B1595 cm^{-1}) and a high-intensity defect related mode (D-band, B1320 cm^{-1}) due to the curved structure and the presence of amorphous carbon inside the cluster.[16] The relative intensity between the D- and G-bands (*i.e.* the I_D/I_G ratio, 1.04 for

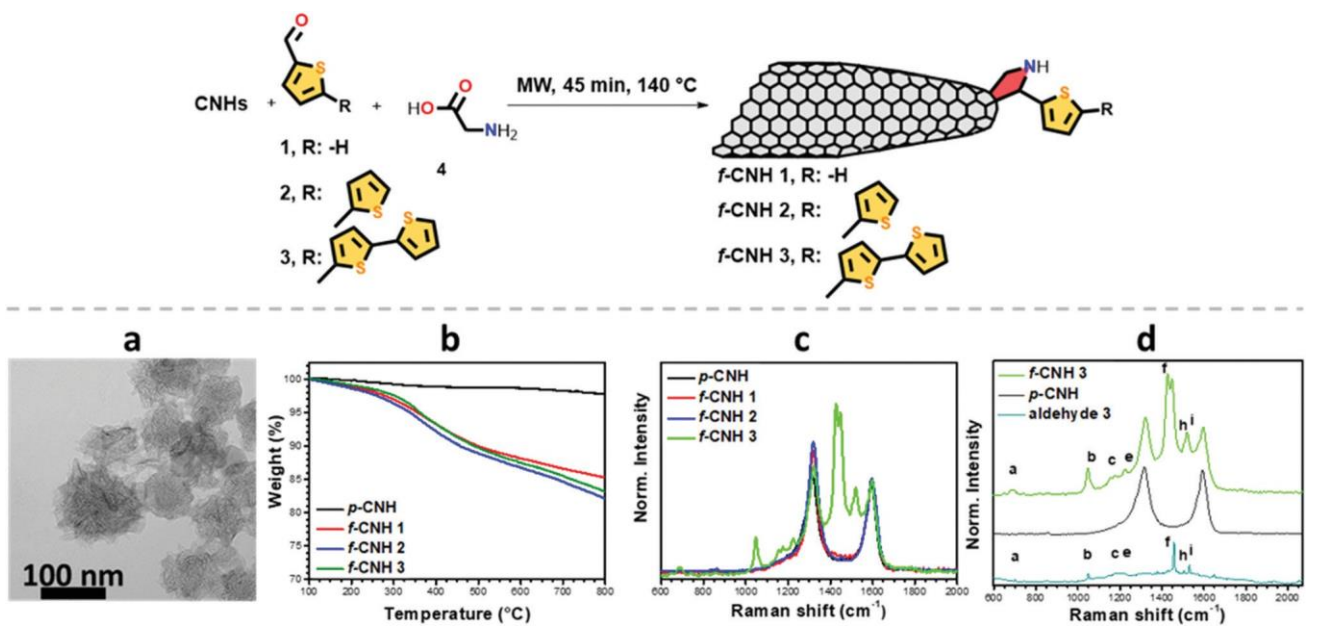

Fig. 1 (Top) Synthesis of f-CNHs. (Bottom) Characterization of f-CNHs showing (a) the TEM image of f-CNH 3, and (b) TGA and (c) Raman spectra of all derivatives; (d) comparison of the Raman spectra with the spectrum of aldehyde 3. Letters in picture d are linked to signals that are denoted in the text. Similar results were obtained when sarcosine was used as amino acid (Fig. S2 ESI†).

p-CNH) increased in all cases and was 1.32 for f-CNH 1 (one thiophene unit), 1.42 for f-CNH 2 (two thiophene units) and 1.16 for f-CNH 3 (three thiophene units). According to the Raman spectra and TGA, the degree of functionalization decreased when the number of thiophene units increased. This effect is likely due to the steric hindrance and the different melting points of the aldehydes (*i.e.* liquid at room temperature, 55–58 ıC, and 141 ıC for aldehydes 1, 2 and 3, respectively), which is markedly important under solvent-free conditions.

Outstandingly, the Raman spectrum of f-CNH 3 displayed bands related to p-CNH and some unexpected additional bands. Most of these bands were attributed to the grafted terthienyl moiety in comparison with the Raman spectrum of aldehyde 3, which revealed a significant Raman enhancement (Fig. 1d). The sharp and high intensity band at 1427 cm^{-1}, denoted as f, could be useful in CNH-based multi-color Raman imaging. To gain insight into the enhancement phenomenon, several experimental and *in silico* investigations were performed.

Firstly, p-CNHs were non covalently functionalized with aldehyde 3 (control-CNHs) to evaluate the importance of the nature of the interaction (*i.e.* covalent *vs.* supramolecular) (Fig. S3, ESI†). Control-CNHs were prepared following a protocol reported by some of us.[11] The Raman spectrum of the control-CNHs showed a negligible trace of aldehyde 3. The low Raman signal of the supramolecular derivative (control-CNHs) in comparison with f-CNH 3 ruled out that the enhanced Raman modes are due to the adsorbed aldehyde molecules. Secondly, CNTs, chosen as the unidimensional analogue of CNHs, were covalently functionalized using glycine and aldehyde 3 (f-CNT 3) to assess the effect of the carbon nanostructure morphology. TGA and Raman spectroscopy confirmed the functionalization; however, the enhancement of Raman bands was not observed (Fig. S4, ESI†).

DFT calculations were implemented to understand the molecular and electronic structure of the functionalized nanomaterials. In agreement with previous DFT studies,[17] larger binding energies were obtained for the sites close to the cone tip when compared to the lateral configurations (Fig. S5, ESI†). Therefore, the tip configuration was chosen as a reference for the remaining work.

The theoretical Raman spectrum of aldehyde 3 nicely predicted the most intense bands experimentally observed and helped in their assignments (Fig. 2). The band at 1457 cm^{-1} (denoted as f) is ascribed to the in-phase $C_a{=}C_b$ stretching vibration delocalized along the whole p-conjugated oligothiophene backbone calculated at 1442 cm^{-1} and the bands at 1506 and 1531 cm^{-1} (denoted as h and i, and calculated at 1495 and 1518 cm^{-1}, respectively) are attributed to the out-of-phase $C_a{=}C_b$ stretching vibration localized in the internal and external thiophene units, respectively (see their corresponding eigenvectors in Fig. S6, ESI†). Importantly, when analysing the theoretical Raman spectrum of f-CNH 3, besides the bands associated to the D and G modes, a very intense band predicted at 1456 cm^{-1} (band f) emerged, which is ascribed to the collective $C_a{=}C_b$ stretching vibration of the terthienyl unit (see the eigenvector in Fig. 2b). It is interesting to note that

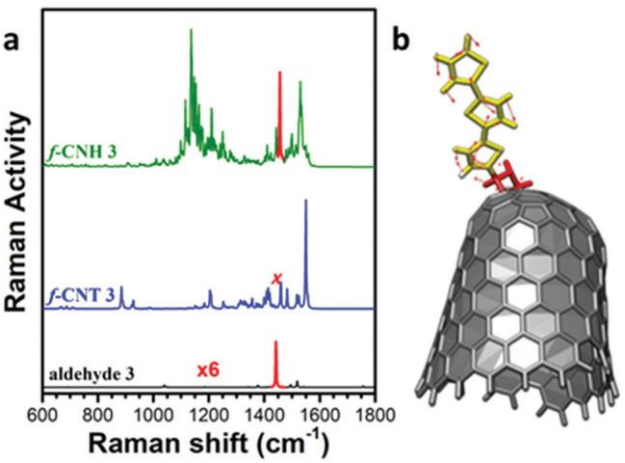

Fig. 2 (a) Theoretical Raman spectra of aldehyde 3, f-CNT 3 and f-CNH 3. Note that the spectrum of aldehyde 3 has been amplified by a factor of 6. (b) Eigenvector associated with the normal mode calculated at 1456 cm^{-1} (band f, highlighted with a red line in the spectrum) for f-CNH 3.A comprehensive table with the experimental and calculated bands (Table S1, ESI†) and the experimental enhancement (Fig. S7, ESI†) for f-CNH 3 are reported in the ESI.†

the Raman activity of the band f is even larger than that associated with the G band in f-CNH 3, and also six times larger when compared with the homologue $C_a{=}C_b$ stretching vibration calculated in aldehyde 3. However, in contrast to the enhancement observed in CNHs, no selective Raman intensification was observed in the analogues f-CNT 3 (Fig. 2a).

Our calculations showed that the relative orientation of the terthienyl unit with respect to the cone tip is crucial for the selective enhancement of the Raman bands. For instance, the largest Raman activity of the collective $C_a{=}C_b$ stretching modes of the terthienyl unit was observed for the configuration where the grafted molecule is largely bent towards the cone tip (491) (denoted as tip 2 configuration in Fig. S3 and S8, ESI†). As seen in Fig. 3a and b, a HOMO–LUMO gap decrease of 0.30 eV was found in f-CNH 3 with tip configurations as compared to the non-functionalized p-CNH; this was associated to the HOMO destabilization and the LUMO stabilization upon functionalization on the conical tip. Note that the HOMO displayed a larger electron density around the lateral surface of CNH and the LUMO was mostly located on the pentagons of the conical tip linked to the pyrrolidine unit, thus suggesting a certain amount of charge-transfer towards the conical tip of f-CNH 3. This is in good accordance with the Mulliken atomic charge distribution that indicated that the terthienyl units are positively charged, while the CNHs are negatively charged (Fig. 3c). The change in the C–C bond length alternation (BLA) pattern of the pyrrolidine units from positive to negative values when the units are attached to CNHs is a consequence of the intramolecular charge-transfer from the oligothienyl spine towards the CNH conical tip (see Table S2, ESI†). In contrast, the HOMO–LUMO gap and the HOMO and LUMO wavefunctions of CNTs are slightly affected upon functionalization (Fig. 3); this is in agreement with the calculated atomic charge distribu-tion and BLA values (Table S3, ESI†) that indicate an absence of

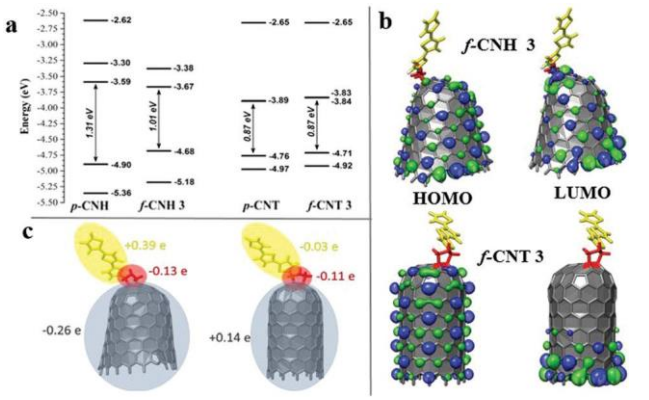

Fig. 3 (a) DFT-calculated molecular orbital energies (M06-2X/6-31G** level) for p-CNHs, f-CNH 3, p-CNT and f-CNT 3. (b) Topologies of the frontier molecular orbitals and (c) Mulliken atomic charges on different molecular domains for f-CNH 3 and f-CNT 3.

charge-transfer character in this particular case from the oligothienyl backbone towards CNTs.

Interestingly, the amount of charge-transfer towards the conical tip was considerably less pronounced for CNHs functionalized with one or two thiophene units (Fig. S9 and S10, ESI†). This effect results in a decrease of the selective enhancement of the Raman scattering of the collective C=C stretching modes associated to the oligothiophene backbone when comparing f-CNH 1 and f-CNH 2 with f-CNH 3 (Fig. S11, ESI†).

Thus, the spectral Raman enhancement observed in f-CNH 3 can be attributed to the following two factors: (i) the strong amplification of the electromagnetic fields near the conical-end of CNHs; note that it is well known that pentagons denote defects within the surrounding aromatic hexagonal network and preferential reactivity to cycloadditions is observed at the conical-tip of CNHs;[18] and (ii) the effect of chemical binding which is mostly related to changes in the electronic structure of the terthiophene unit and their relative orientation to the CNH surface.[19] In addition, the UV-spectroscopic characterization of f-CNH 3 and the remaining functionalized nanocarbons excluded any resonance Raman effect observed. f-CNH 3 and f-CNT 3 displayed a broad absorbance band between ~330 nm and ~530 nm attributed to the terthienyl unit, while the rest of the materials displayed no bands related to the thienyl units (Fig. S12, ESI†).

In conclusion, CNHs functionalized with oligothiophene units were synthesized under microwave irradiation and solvent-free conditions. The Raman spectra of f-CNH 3 exhibited extraordinary properties barely described for carbon nanostructures. To the best of our knowledge, this is the first example reported in the literature where covalent functionalization of this category of materials induces SERS activity. These findings open a new window for the implementation of CNHs in Raman imaging. *In silico* investigations helped us to rationalize the observed Raman enhancement, which was attributed to the intensification of the electromagnetic fields at the tips of f-CNH 3 accompanied by a change of the CNH electronic structure upon functionalization. We consider that the present work will help in better understanding the Raman fingerprint of upcoming functionalized carbon nanostructures and motivate the development of CNH-based Raman applications.

This work was supported by the Iberdrola Foundation (CONV120313), the Spanish Ministerio de Economía y Competitividad (CTQ2017-88158-R), the Junta de Comunidades de Castilla-La Mancha (SBPLY/17/180501/000204) and FEDER-JCCM (UNCM13-1E-1663). The work at the University of Málaga was funded by the MICINN (PID2019-110305GB-I00) and Junta de Andalucía (P09FQM-4708) projects. M. I. L. acknowledges MINECO for her Juan de la Cierva-formación grant (FJCI-2016-29593). The authors acknowledge the computer resources, technical expertise, and assistance provided by the Supercomputing and Bioinformatics centre of the University of Malaga.

Conflicts of interest

There are no conflicts to declare.

Notes and references

1 J. Langer, *et al.*, *ACS Nano*, 2020, **14**, 28–117.
2 X. Wang, C. Wang, L. Cheng, S. T. Lee and Z. Liu, *J. Am. Chem. Soc.*, 2012, **134**, 7414–7422.
3 Z. Liu, X. Li, S. M. Tabakman, K. Jiang, S. Fan and H. Dai, *J. Am. Chem. Soc.*, 2008, **130**, 13540–13541.
4 X. Ling, L. Xie, Y. Fang, H. Xu, H. Zhang, J. Kong, M. S. Dresselhaus, J. Zhang and Z. Liu, *Nano Lett.*, 2010, **10**, 553–561.
5 G. McNay, D. Eustace, W. E. Smith, K. Faulds and D. Graham, *Appl. Spectrosc.*, 2011, **65**, 825–837.
6 G. Bodelón, V. Montes-García, V. López-Puente, E. H. Hill, C. Hamon, M. N. Sanz-Ortiz, S. Rodal-Cedeira, C. Costas, S. Celiksoy, I. Pérez-Juste, L. Scarabelli, A. La Porta, J. Pérez-Juste, I. Pastoriza-Santos and L. M. Liz-Marzán, *Nat. Mater.*, 2016, **15**, 1203–1211.
7 S. Feng, M. Cristina dos Santos, B. R. Carvalho, R. Lv, Q. Li, K. Fujisawa, A. L. Elías, Y. Lei, N. Perea-López, M. Endo, M. Pan, M. A. Pimenta and M. Terrones, *Sci. Adv.*, 2016, **2**, 1–13.
8 G. Hong, S. Diao, A. L. Antaris and H. Dai, *Chem. Rev.*, 2015, **115**, 10816–10906.
9 J. Bartelmess, S. J. Quinn and S. Giordani, *Chem. Soc. Rev.*, 2015, **44**, 4672–4698.
10 N. Karousis, I. Suarez-Martinez, C. P. Ewels and N. Tagmatarchis, *Chem. Rev.*, 2016, **116**, 4850–4883.
11 D. Iglesias, J. Guerra, M. V. Gómez, A. M. Rodríguez, P. Prieto, E. Vázquez and M. A. Herrero, *Chem. – Eur. J.*, 2016, **22**, 11643–11651.
12 V. S. Tiwari, T. Oleg, G. K. Darbha, W. Hardy, J. P. Singh and P. C. Ray, *Chem. Phys. Lett.*, 2007, **446**, 77–82.
13 L. Litti, J. Reguera, F. J. Garciá De Abajo, M. Meneghetti and L. M. Liz-Marzán, *Nanoscale Horiz.*, 2020, **5**, 102–108.
14 C. Cioffi, S. Campidelli, F. G. Brunetti, M. Meneghetti and M. Prato, *Chem. Commun.*, 2006, 2129–2131.
15 N. Rubio, M. A. Herrero, M. Meneghetti, Á. Díaz-Ortiz, M. Schiavon, M. Prato and E. Vázquez, *J. Mater. Chem.*, 2009, **19**, 4407–4413.
16 S. Utsumi, H. Honda, Y. Hattori, H. Kanoh, K. Takahashi, H. Sakai, M. Abe, M. Yudasaka, S. Iijima and K. Kaneko, *J. Phys. Chem. C*, 2007, **111**, 5572–5575.
17 I. D. Petsalakis, G. Pagona, N. Tagmatarchis and G. Theodorakopoulos, *Chem. Phys. Lett.*, 2007, **448**, 115–120.
18 S. Park, D. Srivastava and K. Cho, *Nano Lett.*, 2003, **3**, 1273–1277.
19 J. C. Charlier and G. M. Rignanese, *Phys. Rev. Lett.*, 2001, **86**, 5970–5973.

Electronic Supplementary Information

Microwave-assisted functionalization of carbon nanohorns with oligothiophenes units with SERS activity

Daniel Iglesias,[a] Javier Guerra,[b] María Isabel Lucío,[c] Rafael C. González-Cano,[d] Juan T. López Navarrete,[d] M. Carmen Ruiz Delgado,[d] Ester Vázquez[e,f], M. Antonia Herrero[e,f]

a. Université de Strasbourg, CNRS, ISIS, 8 allée Gaspard Monge, 67000 Strasbourg, France.
b. Facultad de Ciencias, Universidad de Valladolid, 47011, Valladolid, Spain
c. Instituto Interuniversitario de Investigación de Reconocimiento Molecular y Desarrollo Tecnológico (IDM), Universitat Politècnica de València, Universitat de València, Camino de Vera s/n, 46022 Valencia, Spain.
d. Department of Physical Chemistry, University of Málaga, Campus de Teatinos s/n, Málaga 29071, Spain.
e. Facultad de Ciencias y Tecnologías Químicas, Universidad de Castilla-La Mancha (UCLM), 13071 Ciudad Real, Spain
f. Instituto Regional de Investigacion Científica Aplicada (IRICA), 13071 Ciudad Real, Spain

Table of contents

1. General Information

1.1. Materials

All chemicals and solvents were purchased from commercial suppliers and used without prior purification. Carbon nanohorns were purchased at Carbonium s.r.l. Single-walled carbon nanotubes were purchased from Carbon Nanotechnologies Inc. (HiPco® Single-Wall CarbonNanotubes, lot number R0513).

1.2. Methods

Thermogravimetric analyses were recorded with a thermogravimetric analyzer Q50 (TA Instruments). The analyses were performed under N_2 from 100°C to 900 °C by using a 10 °C min^{-1} ramp.

Raman spectroscopy was carried out in a Renishaw InVia microspectrometer equipped with a high-resolution grating (2400 grooves cm^{-1}), a confocal microscope and a 2D-CCD camera. All samples were focused with a ×100 lens and were excited with a red laser (633 nm). The power of the laser was kept under 0.25 mW to avoid damaging the sample. All the reported spectra correspond to the average of several data points to assure the homogeneity of the samples.

UV-Vis spectroscopy was performed on a Varian Cary 5000 spectrophotometer using 1 cm path-length quartz cuvettes. Carbon nanostructures (1 mg) were bath-ultrasonicated in $CHCl_3$ (100 ml) for 15 min before the acquisition.

Transmission electron microscopy images were collected on a Philips EM 208 microscope operating at 100 kV. The dispersion of the sample was drop-casted on top of carbon film TEM grids that were dried under vacuum before the analysis.

Density Functional theory (DFT) calculations were carried out by means of the Gaussian 09 program.[1] The M06-2X[2] functional with the standard 6-31G** basis set[3,4] were used for the geometry optimizations. The M06-2X functional was chosen because of its ability to describe π–π interactions and estimate the energies of weak intermolecular interactions.[5,6] All geometrical

parameters were allowed to vary independently apart from planarity of the rings and no symmetry constraints were imposed during the optimization process. On the resulting ground-state optimized geometries, harmonic vibrational frequencies and Raman intensities were calculated analytically at M06-2X/3-21* level. The more widely used B3LYP[7] was also used to evaluate the ground-state geometries and Raman frequencies of carbon nanohorns. In general, the results (*i.e.*, Raman frequencies and intensities) were very similar when compared to those obtained at the B3LYP level. Molecular orbitals were rendered from geometry optimizations outputs with Chimera 1.11.2 software.[8]

We started with a CNH structure consisting of 360 carbon atoms terminated by 24 hydrogen atoms proposed by Dos Santos *et al.*[9] This conformation where the pentagons set apart one from another to avoid pentagon-pentagon adjacencies was the most stable conformation found among several topologies with different relative positions of the five pentagons existing in the conical tip. This 360-carbon atom model is however far too large for a systematic DFT study, therefore we restricted our model by removing the three outmost strips of 6-membered rings from this previous model resulting in a model containing 214 carbon atoms, terminated by 20 hydrogen atoms. Our nanohorn model has a shape with measured cone angles of 19.2° with a diameter of ≈13.2 Å at the wide end. In postulating how terthiophene interacts with the carbon nanohorn, four different conformations were examined considering two different binding sites of the CNH surface (i.e., close to the cone tip and on the lateral face of the nanohorns) and two different orientations of the terthiophene relative to the CNH surface (named as *1* and *2*). The binding energy is calculated for each configuration as the difference between the calculated energy of the functionalized *f*-CNH 3 system minus the sum of the calculated energies for *p*-CNH and the terthiophene-$CHNHCH_2$ fragment (BE = E [*f*-CNH 1]-E[*p*-CNH]-E[terthiophene-$CHNHCH_2$]). The models for *f*-CNH 1 and *f*-CNH 2 were built taken *f*-CNH 3 as a reference model in tip2 configuration.

In order to compare the CNH behaviour with other carbon nanostructure, structure construction of the zig-zag (12,0) Single-Walled Carbon Nanotube (SWCNT) was performed with NanoCap 1.0.1[10] software, by the use of the empirical carbon potential through the use of the Large Atomic/Molecular Massively Parallel Simulator (LAMMPS).[10] We employed a $C_{198}H_{12}$ cluster model, to represent an one-capped CNT. The boundaries of the nanotube were saturated with

hydrogen atoms, which is a typical procedure for covalent materials. Substitution pattern of the terthiophene on the CNT was built following two non-equivalent placings on the CNT cap (tip1 and tip2) and wall (lateral1 and lateral2), analogously to *f*-CNH 3.

2. Experimental protocols

2.1. Functionalization of carbon nanohorns

The functionalization was carried out following a previously reported protocol.[11] In a microwave quartz vessel, 25 mg of pristine CNHs, glycine (4) (50 mg, 0.66 mmol) and the corresponding aldehyde (1-3) (0.66 mmol) were ultrasonicated in CH_2Cl_2 (10 mL) for 5 min. After ultrasonication, the solvent was removed using a nitrogen stream. The vessel was sealed and introduced in a monomode microwave reactor. The reaction was irradiated for 45 min. The crude was cooled down to room temperature and then suspended in CH_2Cl_2 (75 mL) and sonicated for 5 min. The resulting dispersion was filtered through a Millipore Membrane (JGWP 0.2 µm). The black solid collected from the filter was purified by cycles of ultrasonication/filtration in different solvents: (i) methanol/HCl (37%) 3/1 (100 mL); (ii) methanol (100 mL); (iii) dimethylformamide (200 mL); and (iv) CH_2Cl_2 (75 mL). The product was eventually dried under vacuum affording the desired material as black solids (*f*-CNH 1 (26 mg), *f*-CNH 2 (22 mg) and *f*-CNH 3 (27 mg)). Analogously, *f*-CNH 3 was prepared using sarcosine instead of glycine.

2.2. Calculation of the degree of functionalization

The degree of functionalization is calculated using the data extracted from the thermograms. Below, the calculation of the degree of functionalization for *f*-CNH 3 is shown as an example.

1. From the thermogram, the difference of weight loss between p-CNH and *f*-CNH 3 at 550 °C is attributed to the functionalization:

$$99.7\ \% - 86.7\% = 13\ \%\ of\ functional\ molecule$$

2. Therefore,

$$\frac{0.13\ g\ of\ functional\ molecule}{1\ g\ of\ f-CNH\ 3}$$

3. Considering the molecular weight of the grafted function, 290 g/mol for *f*-CNH 3, the number of micromoles of functional groups per gram of CNH can be calculated:

$$\frac{0.13\ g\ of\ functional\ molecule}{1\ g\ of\ f-CNH\ 3} \times \frac{1\ mol\ of\ functional\ molecule}{290\ g\ functional\ molecule} \times \frac{10^6 \mu mol}{1\ mol} = 448\ \mu mol/g$$

2.3. Synthesis of control-CNH

The functionalization was carried out following a previously reported protocol.[12] Pristine CNHs (10 mg) and 2,2':5',2''-terthiophene-5-carboxaldehyde 3 (40 mg) were ultrasonicated in $CHCl_3$ (10 mL) for 15 min. The resulting dispersion was stirred for 48 h at room temperature. After that, the crude was filtered through a Millipore Membrane (JGWP 0.2 µm). The black solid collected from the filter was purified by cycles of ultrasonication/filtration in different solvents (*o*-dichlorobenzene (200 mL), $CHCl_3$ (100 mL), CH_2Cl_2 (100 mL) and diethyl ether (50 mL)). Afterwards the product was dried under vacuum affording 8 mg of composite.

2.4. Functionalization of carbon nanotubes

f-CNT 3 (21 mg) was prepared following the same procedure applied for *f*-CNH 3 but using CNTs instead of CNHs.

3. Supplementary figures

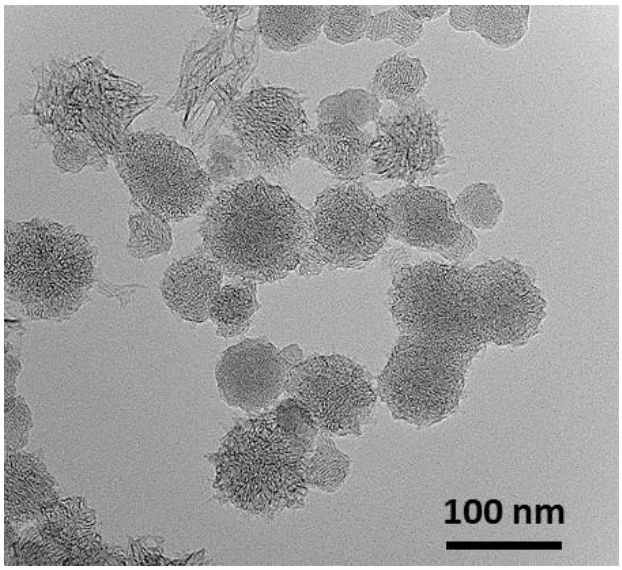

Figure S 1. Transmission microscopy image of *p*-CNH.

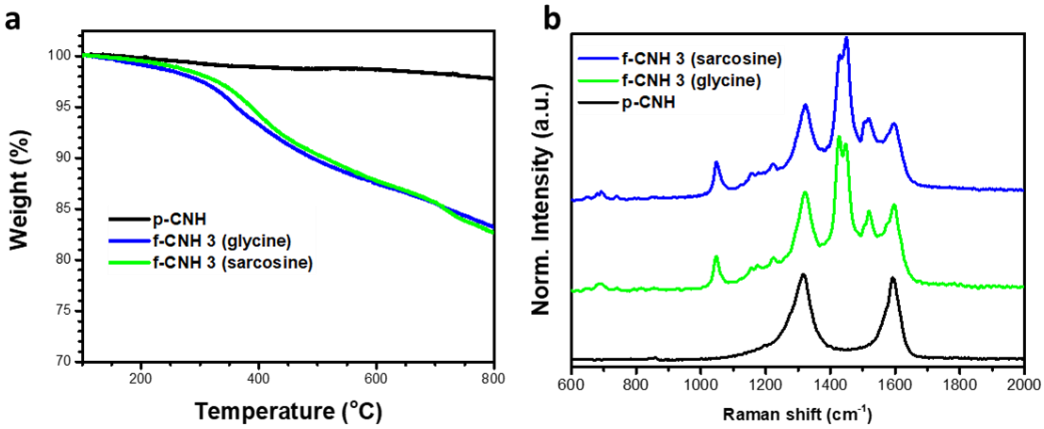

Figure S 2. (a) TGA and (b) Raman characterization of *p*-CNH and *f*-CNH 3 with glycine or sarcosine. The data show that the functionalization and Raman enhancement are analogous in both cases.

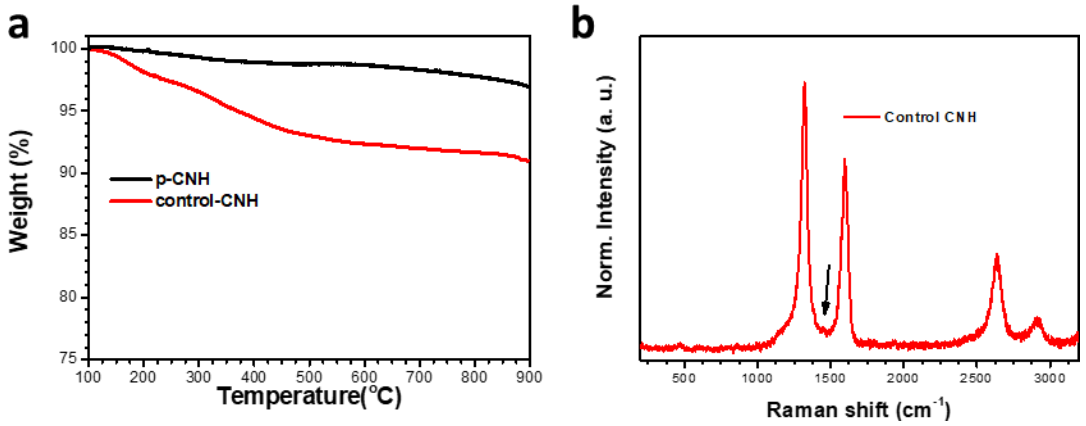

Figure S 3. (a) TGA of *p*-CNH and control-CNH and (b) Raman characterization of control-CNH. The black arrow in (b) indicates the trace of the signal of aldehyde 3.

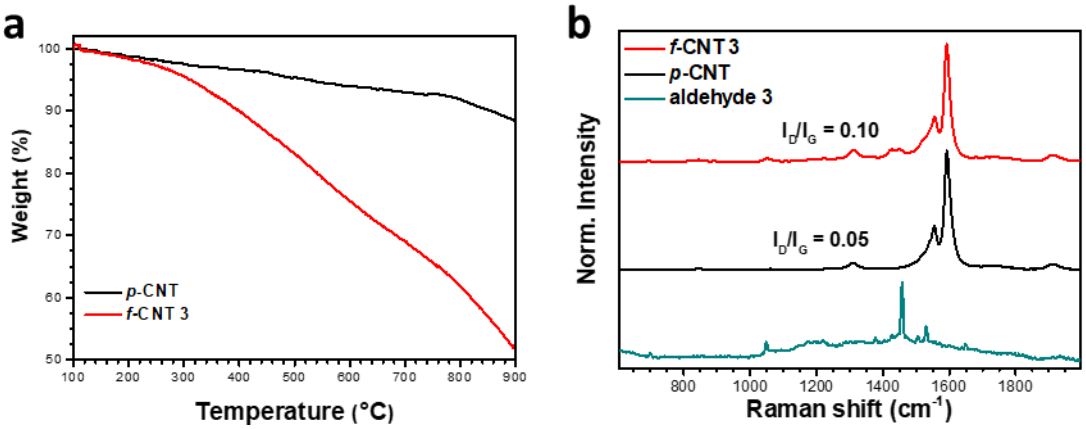

Figure S 4. (a) TGA and (b) Raman characterization of *f*-CNT 3. The Raman of aldehyde 3 was added for the sake of comparison.

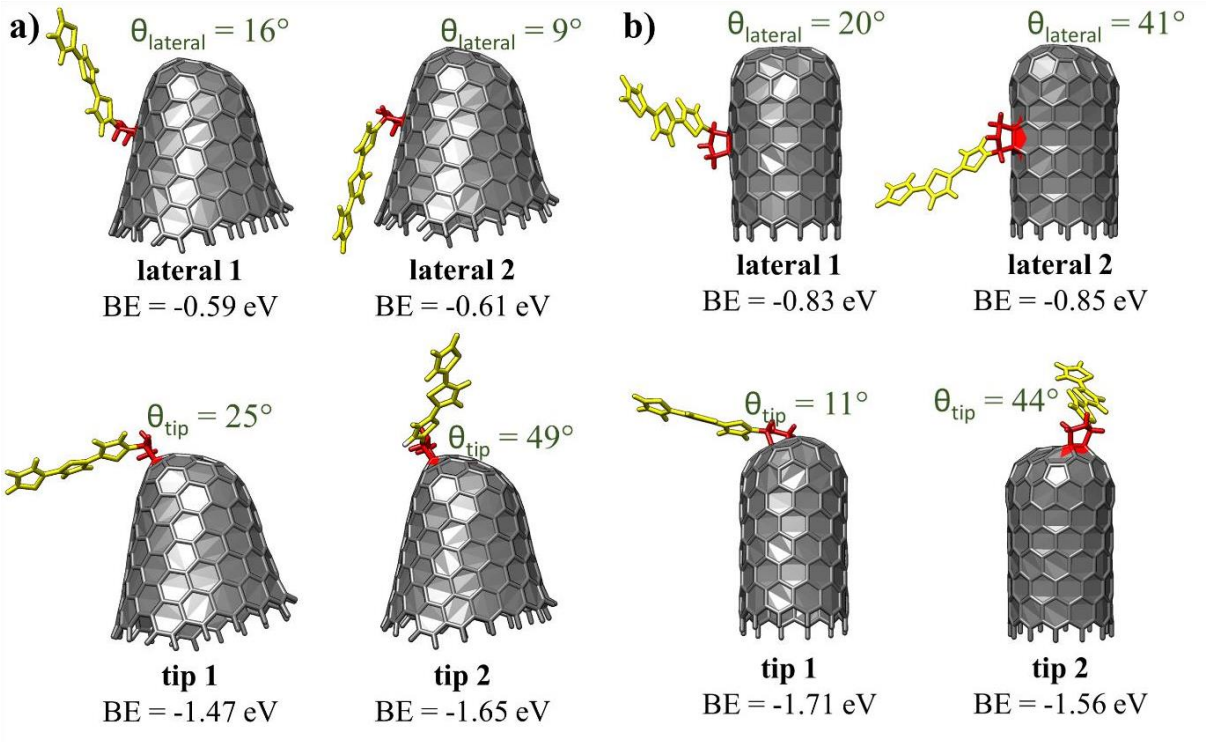

Figure S 5. DFT-optimized geometries of the *f*-CNH 3 (a) and *f*-CNT 3 (b) models in four different configurations calculated at the M06-2X/6-31G** level. Binding energy (BE) values and the angles between the planes formed by the terthienyl unit and the conical tip (Θ_{tip}) and by the terthienyl unit and the lateral surface ($\Theta_{lateral}$) are also shown.

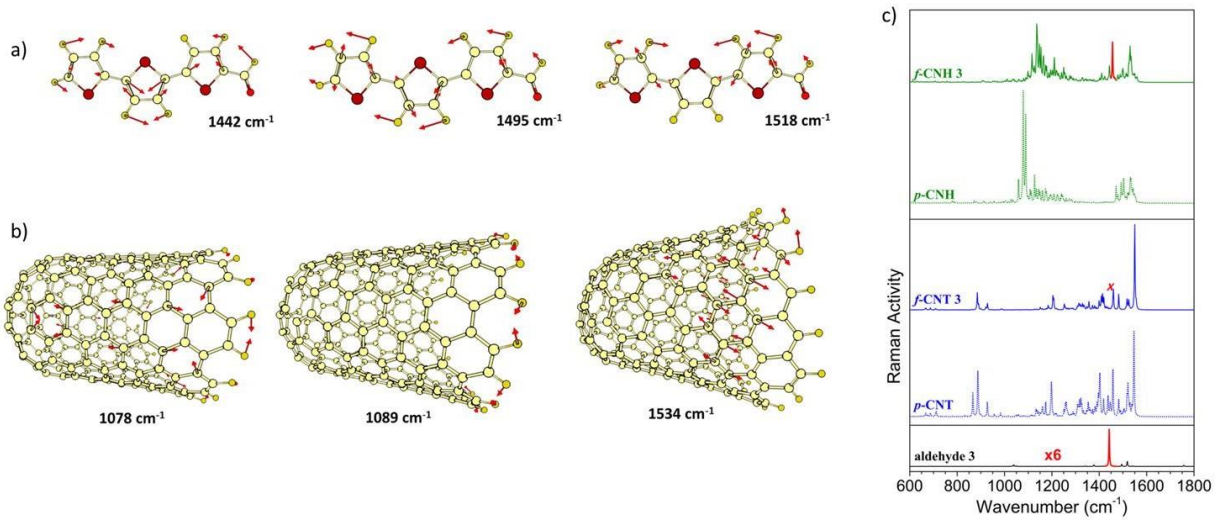

Figure S 6. M06-2X/3-21G* vibrational eigenvectors associated with the most outstanding Raman features of (a) aldehyde 3 and (b) *p*-CNH. (c)Theoretical Raman spectra of aldehyde 3, *p*-CNH, *p*-CNT and functionalized *f*-CNH 3, *f*-CNT 3 in tip 2 configuration.

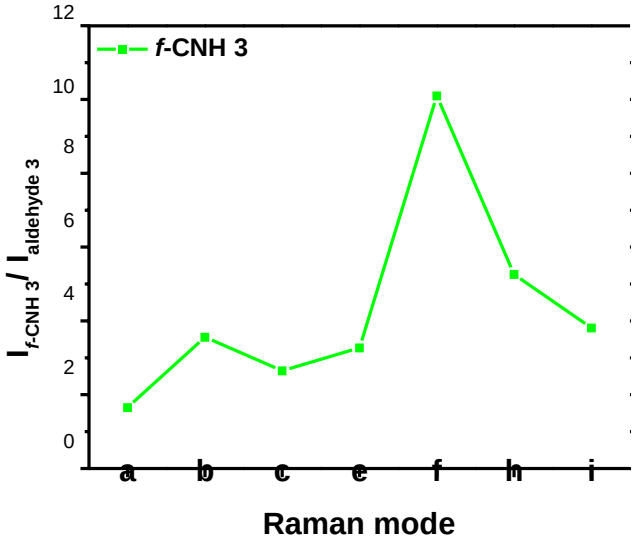

Figure S 7. Relative Raman Intensity of the aldehyde 3 deposited on the SiO_2/Si compared to the derivative *f*-CNH 3. Note that the reported Raman enhancement is underestimated as the amount of terthienyl units in *f*-CNH 3 is smaller than in pure aldehyde 3.

Table S 1. Raman shifts of the characteristic peaks found in the spectra and the corresponding calculated wavelengths.

band	aldehyde 3 exp.	aldehyde 3 theo.	*f*-CNH 3[a] theo.	*f*-CNH 3 exp.	DESCRIPTION	SYMBOL
a	700	691	688	692	CS in-plane bending	δ (CS)
b	1048	1039	1046	1048	Out-of-phase ring C-H in-plane bending	δ_a (CH)
c	1152	1185	1189	1156	C-C in-plane bending	δ (CC)
e	1219	1236	1203	1223	In-phase ring C-H in-plane bending	δ_s (CH)
f	1457	1442	1456	1450	In-phase C=C stretching	υ_s (C=C)
h	1506	1495	1500	1506	Out-of-phase C=C stretching	υ_a (C=C)
i	1531	1518	1529	1520	Out-of-phase C=C stretching	υ_a (C=C)

[a] Calculated in tip 2 *configuration*.

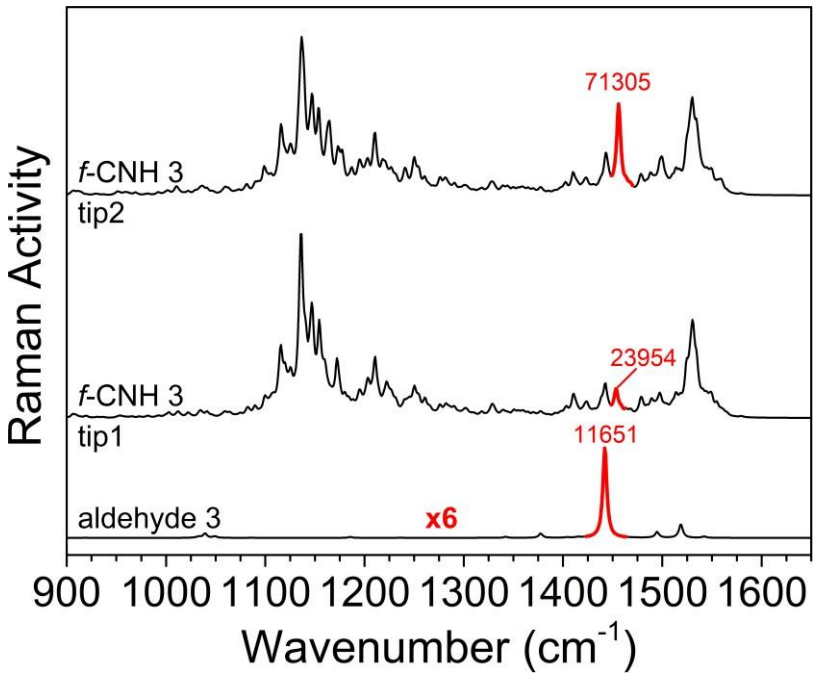

Figure S 8. Theoretical Raman spectra of functionalized *f*-CNH 3 in tip 1 and tip 2 configurations (see Figure S3). The bands associated with the C=C/C-C stretching mode localized on the terthiophene group are denoted in red; the calculated Raman scattering activity values (in A^4/AMU) associated to this mode are also shown.

Table S 2. DFT calculated bond-length alternation (BLA) values and dihedral angles for the aldehyde) and functionalized *f*-CNH 3. The values in parentheses correspond to a terthiophene linked to a pyrrolidine unit.

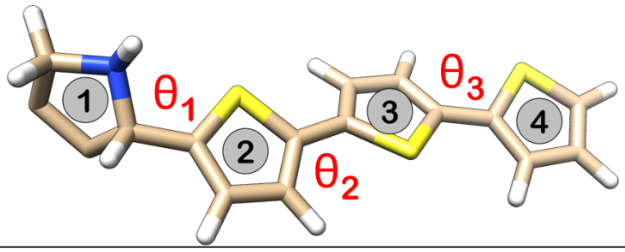

BLA values (Å)

rings	terthiophene	*f*-CNH 3			
		tip1	*tip2*	*lateral1*	*lateral2*
1	(0.005)	-0.014	-0.018	0.027	0.019
2	0.038 (0.057)	0.053	0.054	0.052	0.052
3	0.046 (0.049)	0.048	0.048	0.048	0.045
4	0.057 (0.057)	0.057	0.057	0.057	0.059

Dihedral angles (°)

θ	terthiophene	*f*-CNH 3			
		tip1	*tip2*	*lateral1*	*lateral2*
θ_1	1 (92)	114	-91	-86	84
θ_2	163 (157)	161	157	163	165
θ_3	158 (157)	158	157	159	171

Table S 3. DFT calculated bond-length alternation (BLA) values and dihedral angles for the aldehyde 3 and functionalized *f*-CNT 3. The values in parentheses correspond to a terthiophene linked to a pyrrolidine unit.

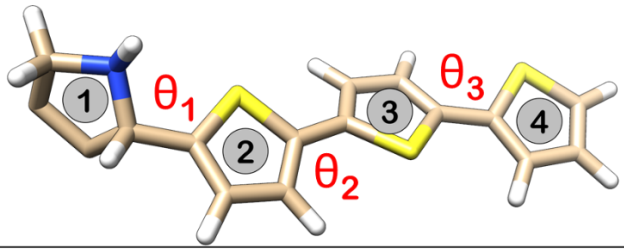

BLA values (Å)

rings	terthiophene	*f*-CNT 3			
		tip1	*tip2*	*lateral1*	*lateral2*
1	(0.005)	0.036	0.033	0.003	0.002
2	0.038 (0.057)	0.054	0.056	0.053	0.052
3	0.046 (0.049)	0.049	0.048	0.048	0.048
4	0.057 (0.057)	0.058	0.057	0.057	0.057

Dihedral angles (°)

θ	terthiophene	*f*-CNT 3			
		tip1	*tip2*	*lateral1*	*lateral2*
θ_1	1 (92)	87	107	119	45
θ_2	163 (157)	158	165	160	163
θ_3	158 (157)	158	158	159	158

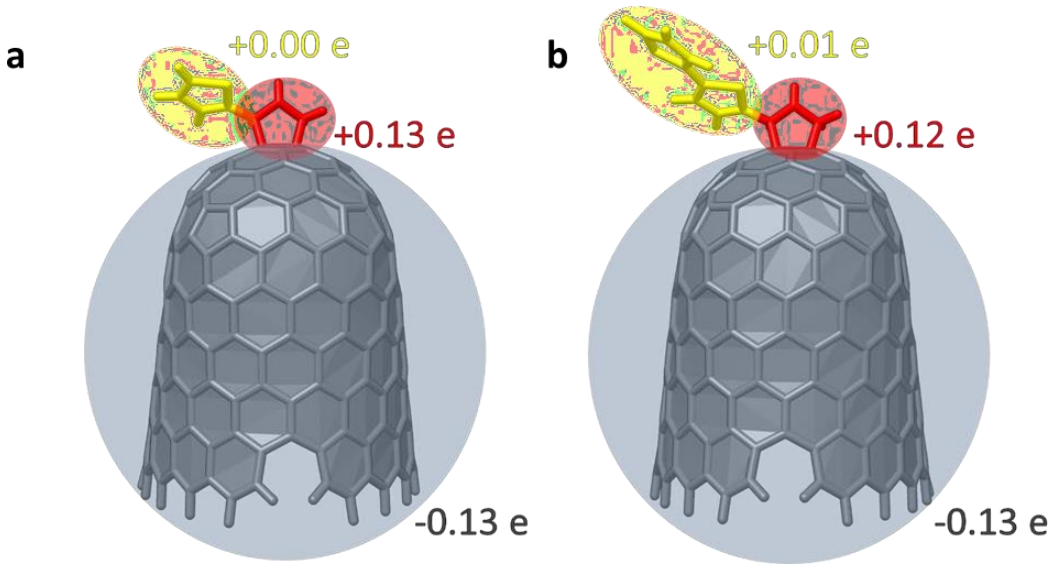

Figure S 9. Mülliken atomic charges on different molecular domains for *f*-CNH 1 and *f*-CNH 2 in tip 2 configuration.

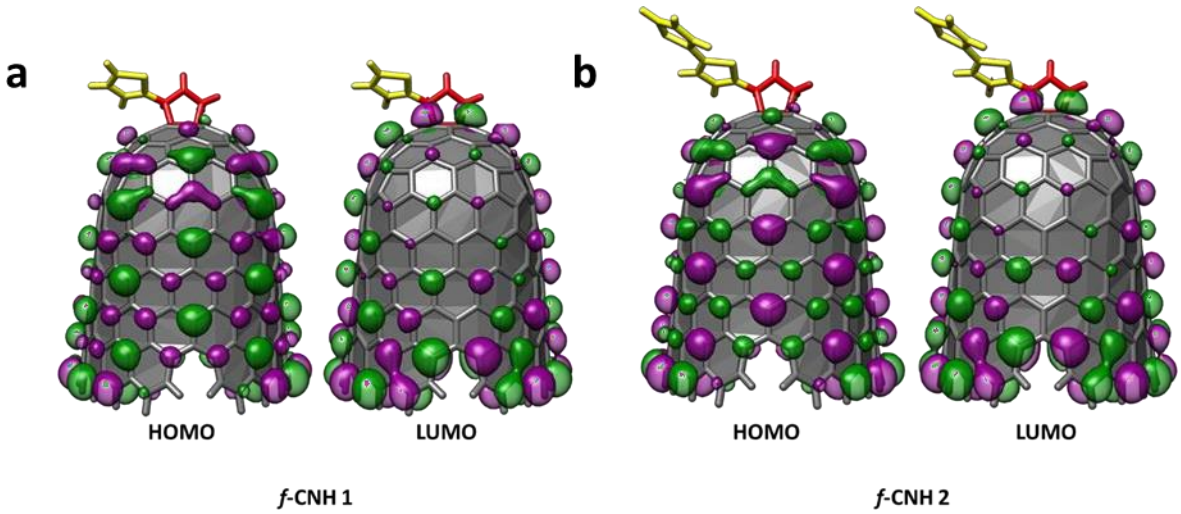

Figure S 10. Topologies of the frontier molecular orbitals of functionalized *f*-CNH 1 and *f*-CNH 2 in tip 2 configuration.

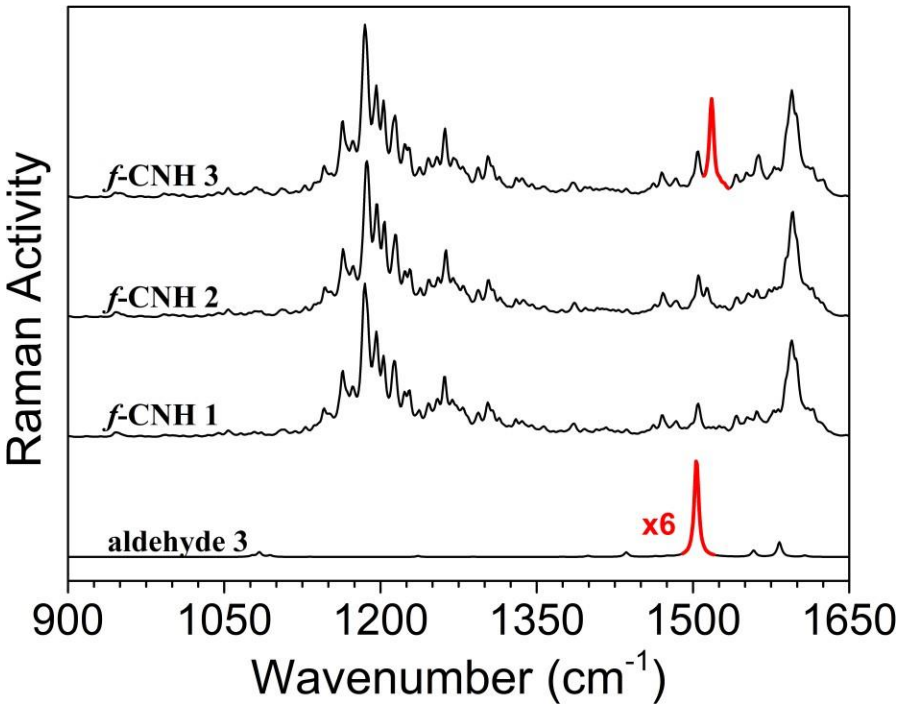

Figure S 11. Theoretical Raman spectra (M06-2X/3-21G*) of functionalized *f*-CNH 1, *f*-CNH 2 and *f*-CNH 3 in tip 2 configuration. The bands associated with the C=C/C-C stretching mode localized on the oligothiophene group are denoted in red.

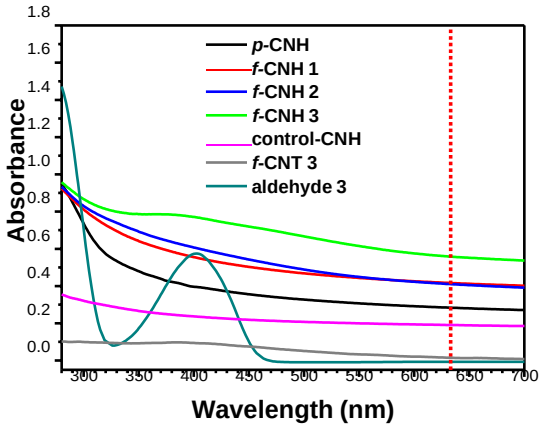

Figure S 12. UV-Vis spectra of the most relevant materials in $CHCl_3$ (0.01 mg/ml). The dotted line indicated the position of the red laser (633 nm) used for the Raman analysis.

4. References

1 M.J.Frisch,G. W. Trucks, H. B. Schlegel, G. E. Scuseria, M. A. Robb, J. R. Cheeseman, G. Scalmani, V. Barone, G. A. Petersson, H. Nakatsuji, X. Li, M Caricato, A. V. Marenich, J. Bloino, B. G. Janesko, R. Gomperts, B. Mennucci, H. P. Hratchian, J. V. Ortiz, J. L. Izmaylov, J.
L. Sonnenberg, Williams, F. Ding, F. Lipparini, F. Egidi, J. Goings, B. Peng, A. Petrone, T. Henderson, D. Ranasinghe, V. G. Zakrzewski, J. Gao, N. Rega, G. Zheng, W.Liang, M. Hada, M.Ehara, K. Toyota, R. Fukuda, J. Hasegawa, M. Ishida, T. Nakajima, Y. Honda, O. Kitao, H. Nakai,T.Vreven, K. Throssell, J. A. Jr. Montgomery, J. E. Peralta, F. Ogliaro, M. J. Bearpark, M. J.; Heyd, E. N. Brothers, K. N. Kudin, V. N. Staroverov, T.A. Keith, R. Kobayashi, J. Normand, K. Raghavachari, A. P. Rendell, J. C. Burant, S. S. Iyengar, J. Tomasi, M. Cossi, J. M. Millam, M. Klene, C. Adamo, R. Cammi, J. W. Ochterski, R. L. Martin, K. Morokuma, O. Farkas, J. B. Foresman, D. J. Fox, et al. Gaussian 09, revision C.01; Gaussian Inc.: Wallingford, CT, 2009.

2 Y. Zhao and D. G. Truhlar, *Acc. Chem. Res.*, 2008, **41**, 157–167.

3 W. J. Hehre, D. R and J. A. Pople, *J. Chem. Phys.*, 1972, **56**, 2257.

4 M. M. Francl, W. J. Pietro, W. J. Hehre, J. S. Binkley, M. S. Gordon, D. J. DeFrees and J. A. Pople, *J. Chem. Phys.*, 1982, **77**, 3654−3665.

5 K. E. Riley, M. Pitonak, J. Cerny and P. Hobza, *J. Chem. Theory Comput.*, 2010, **6**, 66–80.

6 I. Badía-Domínguez, A. Pérez-Guardiola, J. C. Sancho-García, J. T. López Navarrete, V. Hernández Jolín, H. Li, D. Sakamaki, S. Seki and M. C. Ruiz Delgado, *ACS Omega*, 2019,**4**, 4761–4769.

7 C. Lee, W. Yang and R. G. Parr, *Phys. Rev. B*, 1988, **37**, 785–789.

8 E. F. Pettersen, T. D. Goddard, C. C. Huang, G. S. Couch, D. M. Greenblatt, E. C. Meng and T. E. Ferrin, *J. Comput. Chem.*, 2004, **25**, 1605–1612.

9 H. F. Dos Santos, L. A. De Souza, W. B. De Almeida and T. Heine, *J. Phys. Chem. C*, 2014,
118, 24761–24768.

10 M. Robinson and N. A. Marks, *Comput. Phys. Commun.*, 2014, **185**, 2519–2526.

11 N. Rubio, M. A. Herrero, M. Meneghetti, Á. Díaz-Ortiz, M. Schiavon, M. Prato and E. Vázquez, *J. Mater. Chem.*, 2009, **19**, 4407–4413.

12 D. Iglesias, J. Guerra, M. V. Gómez, A. M. Rodríguez, P. Prieto, E. Vázquez and M. A. Herrero, *Chem. - A Eur. J.*, 2016, **22**, 11643–11651.